Vol. 16, pp. 28–40 (2019)
doi: 10.2142/biophysico.16.0_28

Biophysics and Physicobiology
https://www.jstage.jst.go.jp/browse/biophysico/

Regular Article

Functional significance of HCM mutants of tropomyosin, V95A and D175N, studied with *in vitro* motility assays

Shuya Ishii[1], Madoka Suzuki[2,3], Shin'ichi Ishiwata[1] and Masataka Kawai[4]

[1]*Department of Physics, Faculty of Science and Engineering, Waseda University, Shinjuku-ku, Tokyo 169-8555, Japan*
[2]*Institute for Protein Research, Osaka University, Suita, Osaka 565-0871, Japan*
[3]*PRESTO, Japan Science and Technology Agency (JST), Kawaguchi, Saitama 332-0012, Japan*
[4]*Department of Anatomy and Cell Biology, College of Medicine, University of Iowa, Iowa City, IA 52242, USA*

Received September 25, 2018; accepted December 18, 2018

The majority of hypertrophic cardiomyopathy (HCM) is caused by mutations in sarcomere proteins. We examined tropomyosin (Tpm)'s HCM mutants in humans, V95A and D175N, with *in vitro* motility assay using optical tweezers to evaluate the effects of the Tpm mutations on the actomyosin interaction at the single molecular level. Thin filaments were reconstituted using these Tpm mutants, and their sliding velocity and force were measured at varying Ca^{2+} concentrations. Our results indicate that the sliding velocity at pCa ≥8.0 was significantly increased in mutants, which is expected to cause a diastolic problem. The velocity that can be activated by Ca^{2+} decreased significantly in mutants causing a systolic problem. With sliding force, Ca^{2+} activatable force decreased in V95A and increased in D175N, which may cause a systolic problem. Our results further demonstrate that the duty ratio determined at the steady state of force generation in saturating [Ca^{2+}] decreased in V95A and increased in D175N. The Ca^{2+} sensitivity and cooperativity were not significantly affected by the mutations. These results suggest that the two mutants modulate molecular processes of the actomyosin interaction differently, but to result in the same pathology known as HCM.

Key words: Hypertrophic cardiomyopathy, tropomyosin mutants, TIRF, optical tweezers, sliding velocity and force

Corresponding author: Masataka Kawai, Department of Anatomy and Cell Biology, 51 Newton Road, University of Iowa, Iowa City, IA 52242, USA.
e-mail: masataka-kawai@uiowa.edu

Hypertrophic cardiomyopathy (HCM) occurs in 1/500 of population [1–8]. Among those affected by HCM, a sudden cardiac death occurs at the rate of 1–2% in young and active adults as well as in elderly population [2,3,6,9]. About 60% of HCM cases are familial diseases and inherited, mainly due to mutations in sarcomeric proteins [1,3,4,6] that include β-myosin heavy chain (gene: *MYH7*), myosin essential light chain (*MYL3*), myosin regulatory light chain *(MYL2)*, myosin binding protein-C (*MYBPC3*), TnC (*TNNC1*), TnI (*TNNI3*), TnT (*TNNT2*), α-tropomyosin (α-Tpm) (*TPM1*), α-actin (*ACTC*), and titin (connectin) (*TTN*) [1,4,6–8,10]. Expression levels of these mutant proteins are variable among patients, hence environmental factors are also involved. Some individuals with a mutation may remain asymptomatic, whereas others with the same mutation experience severe symptoms [1–3,5,10,11]. Even different

◀ ***Significance*** ▶

In vitro motility assay was used to examine regulatory functions of thin filaments that contain tropomyosin mutants V95A or D175N, which are known to cause hypertrophic cardiomyopathy (HCM) in humans. The sliding velocity during relaxation was significantly increased in these mutants compared to wild type (WT) tropomyosin. Ca^{2+}-activatable sliding force decreased in V95A and increased in D175N. The duty ratio determined at the steady state of force generation at saturating [Ca^{2+}] decreased in V95A and increased in D175N. We conclude that HCM mutants of tropomyosin differently modulate molecular processes of the actomyosin interaction.

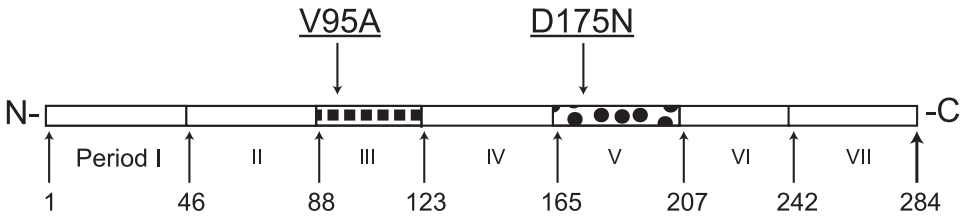

Figure 1 Structure of Tpm. Tpm consists of seven quasi repeats. V95A and D175N are located in period 3 and 5, respectively. Periods 2 and 3 contribute to the positive cooperative effect of Tpm on actin [31,32]. The period 5 is thought to be responsible for TnT interaction [28] and relaxation [32].

mutants can exhibit the same pathogenesis [1,6].

To understand the contractile properties altered by HCM mutations, multi-facial approaches have been made. These are, in the increasing order of complexity: (i) *in vitro* motility assay, (ii) myofibril, (iii) muscle fiber (cell), (iv) transgenic animal model, and (v) human patient study. The approach (i) uses the reconstituted system based on purified proteins, and (ii) and (iii) use a technique of selective removal of endogenous proteins and their replacement with purified proteins [12,13]. (iv) uses animal models in which a single gene is replaced with a mutated one. At this level, myocyte hypertrophy and disarray, and interstitial fibrosis are noticed [14]. (v) is the most difficult and complex, yet the most significant part of investigations on heart diseases. Eventual understanding of the diseases and their treatments must depend on the combined efforts of all of these approaches and disciplines. Our present report is based on approach (i), and aims at understanding the immediate molecular effects that follow a gene alteration and its expression.

A variety of molecular and cellular hypotheses have been proposed to account for the mechanisms leading to HCM: diminished contractility [15,16], irregular formation of myofibril structures [17,18], increased ATP hydrolysis rate and active force [19], altered Ca^{2+}-sensitivity [20–24], incomplete relaxation during diastole [16,25], and diminished myocyte relaxation rate [26]. In the case of α-Tpm, 17 missense mutations are known to cause HCM [7]. A coiled-coil Tpm molecule is composed of seven quasi-repeats or "periods" [27]. Investigations on regional deletion/replacement mutants have suggested that each Tpm period is associated with a function(s) that characterizes the period [28–32]: periods 1 and 7 are essential for the head-to-tail association of neighboring Tpm molecules, periods 2 and 3 play an important role for allosteric activation of actin [31,32], and periods 4-6 are required for the Ca^{2+}-regulatory function [28,32].

In our current study, we evaluated the molecular mechanism of contractile dysfunction caused by human α-Tpm mutants V95A and D175N that are located in periods 3 and 5, respectively (Fig. 1). Following to our previous study on the effects of HCM mutants on force generation using reconstituted muscle fibers [16], we examined the molecular mechanism of contractile dysfunction caused by the Tpm mutants at the single molecular level. We deduced two parameters from the *in vitro* motility assay using optical tweezers: sliding force at the steady state in saturating [Ca^{2+}] and unloaded sliding velocity. We found that the suppression of the actomyosin interaction at low [Ca^{2+}] is insufficient in either Tpm mutant, and the active force is modulated by the mutant. We then propose how the Tpm mutants modulate the duty ratio, thereby the mechanisms of force generation.

Materials and Methods

Purification of proteins

The wild type (WT) and two mutants associated with HCM (V95A and D175N) of human α-Tpm were expressed in *E. coli* as recombinant proteins and purified in Chase laboratory at the Florida State University [33,34]. Because bacterially expressed proteins lack N-terminal acetylation, two extra amino acid residues, Gly-Ser, were attached at the N-terminus to functionally substitute for the acetylation. Two rabbits were purchased from Japan Laboratory Animals, Inc., and used for the present study. Actin and heavy meromyosin (HMM: α-chymotrypsin proteolytic fragment of myosin II) were purified from rabbit white skeletal muscles as described previously [35,36]. All experimental procedures conformed to the "Guidelines for Proper Conduct of Animal Experiments" approved by the Science Council of Japan and were performed according to the "Regulations for Animal Experimentation" at Waseda University. Gelsolin from bovine plasma and bovine ventricular troponin (Tn; a complex of TnI, TnC and TnT) were purified as described previously [37,38]. Bovine samples were obtained as food by-products.

Solutions

F-buffer contained 2 mM $MgCl_2$, 1.5 mM NaN_3, 100 mM KCl, 1 mM dithiothreitol (DTT), 2 mM 3-(*N*-morpholino) propanesulfonic acid (MOPS), and pH adjusted to 7.0. Rigor solution contained 4 mM $MgCl_2$, 1 mM ethylene glycol bis (β-aminoethyl ether) N,N′-tetraacetic acid (EGTA), 25 mM KCl, 10 mM DTT, 25 mM Imidazole-HCl (Im-HCl). Relaxing solution contained 2 mM Na_2ATP (Roche Diagnostics, Indianapolis, IN, USA), 4 mM $MgCl_2$, 1 mM EGTA, 13 mM KCl, 6 mM KH_2PO_4, 10 mM DTT, and 25 mM Im-HCl.

Activating solution was the same as the relaxing solution, except that 1 mM $CaCl_2$ was added (pCa = 5.0). pCa 4.0 solution contained 2 mM Na_2ATP, 4 mM $MgCl_2$, 1 mM EGTA, 1.15 mM $CaCl_2$, 12.6 mM KCl, 6 mM KH_2PO_4, 10 mM DTT, and 25 mM Im-HCl. Solutions in the range of pCa 5.5–9.0 were appropriate mixtures of the relaxing and activating solutions, and pCa 4.5 solution was an appropriate mixture of the pCa 4.0 solution and the activating solution. Except for F-buffer, pH and ionic-strength of these solutions were adjusted to 7.4 and 50 mM, respectively. All chemicals were purchased from Wako Pure Chemical Industries (Osaka, Japan), unless otherwise stated.

Preparation of bead-tailed reconstituted thin filaments

Bead-tailed actin filaments (F-actin) were prepared as previously described [36,39,40]. In brief, polystyrene beads (1.0 μm in diameter, Molecular probes, Eugene, OR, USA) were coated with the mixture of gelsolin and tetra methyl rhodamine-maleimide (Molecular Probes) conjugated with bovine serum albumin (BSA: Sigma-Aldrich, St. Louis, MO, USA) using the carboxyl group at the surface of the beads [36]. Rhodamine-conjugated phalloidin (Molecular Probes) was bound to F-actin, which was then attached to the polystyrene bead through gelsolin. We reconstituted the bead-tailed thin filaments in a test tube (20 μL) starting from the bead-tailed actin filaments (corresponding to 0.6 μM G-actin) in the presence of 0.6 μM Tpm and 0.6 μM Tn. The mixture was incubated for 1 hour on ice [41], followed by *annealing* treatment (45°C, 10 min) to achieve correct head-to-tail interaction between neighboring Tpm molecules along the actin filament [42] and to improve the reproducibility of results. After reconstitution, the samples were stored on ice until used for experiments.

Optical setup

The optical setup used in this study was same as the one described previously [43]. Briefly, the setup was built around an inverted microscope (IX 71, Olympus, Tokyo, Japan). The light from an Nd-YLF laser (T20-BL-106C, 1064 nm, 1W, Spectra-Physics, Santa Clara, CA, USA) was led through the objective lens (Apo TIRF 100X oil-immersion, N.A. = 1.49, Nikon, Tokyo, Japan) to function as optical tweezers. The bright field image using the light from a Xenon lamp (MAX-303, filtered to 710–900 nm, Asahi Spectra, Tokyo, Japan) was monitored by two cameras. One CCD camera (MC-781P; Texas Instruments, Inc., Dallas, TX, USA) recorded the bright field image together with fluorescence image at a video rate of 30 fps. The other high speed camera (IMPERX, Inc., Boca Raton, FL, USA) was used to record at 200 fps for real-time tracking of the position of the trapped bead. Green laser (532 nm, Melles Griot KK, Tokigawa, Saitama, Japan) was used for the total internal reflection fluorescence (TIRF) microscopy, which illuminated only the vicinity of the cover slip surface (~100 nm) specifically exciting the filaments interacting with HMM on the cover slip. Concomitant rhodamine fluorescent light (570–600 nm) from the thin filaments was amplified by an image intensifier (Video Scope international, Ltd., Dulles, VA, USA), and recorded by another CCD camera (EB-CCD, MC681SPD-ROBO, Texas Instruments, Inc.). Bright-field and TIRF images were combined and monitored on the same screen using a multi-viewer (MV-40F, FOR-A, Tokyo, Japan), then recorded in a personal computer (PC) with an eight bit resolution using a custom-built program based on LabVIEW (National Instruments Japan, Tokyo, Japan). All equipment was turned on one hour before experiments to reduce thermal drift.

***In vitro* motility assay**

The protocol to prepare the *in vitro* motility assay was based on our previous report [43] with modifications (Fig. 2). The first drop (20 μL) of HMM solution (30 μg/mL in Rigor solution) was injected from a side of the flow cell and settled for 60 s. In this period the HMM molecules were attached to the collodion-coated surface of the coverslip. The second drop of the HMM solution (20 μL) was injected from the other side of the flow cell and settled for 60 s. Then 20 μL of the experimental solution (Rigor or a pCa solution containing 5 mg/mL BSA) was injected and allowed to settle for 5 min. Finally, 50 μL of the experimental solution containing the bead-tailed F-actin or reconstituted thin filaments (diluted by 1:100 from the one stored) and 1 mg/mL BSA were injected to the flow cell. In experimental solutions for the reconstituted thin filaments, 100 nM excess Tpm and 100 nM excess Tn were added to ensure that Tpm and Tn were bound and saturated on the thin filaments [44]. The experimental solutions also contained 25 mM glucose, 0.22 mg/mL glucose oxidase, and 0.036 mg/mL catalase as the oxygen scavenger system. Finally, two open ends of the flow cell were sealed with nonfluorescent enamel, and the flow cell was placed on the microscope stage. More than two flow cells were used per one condition. All flow cells were studied in less than 45 min to avoid reduction in [ATP]. All experiments were performed at 24 ± 1°C.

Analysis of the sliding velocity of thin filaments

Moving filaments were tracked to determine the unloaded sliding velocity. Because of the previous report that the velocity depends on the total number of cross-bridges interacting with a filament [45], the length of the filament sampled in this study was limited between 2 and 4 μm.

We manually tracked the filaments with a fixed time interval of 67 ms continuously (using image J plugin: Manual Tracking), and calculated the sliding velocity in each 200 ms interval. Then, the data from all the intervals were averaged to deduce the sliding velocity. The interval of 200 ms was chosen to minimize the Brownian motion effect on the sliding velocity [46].

Because of a possible presence of local unevenness of myosin density on the coverslip surface, more than two areas

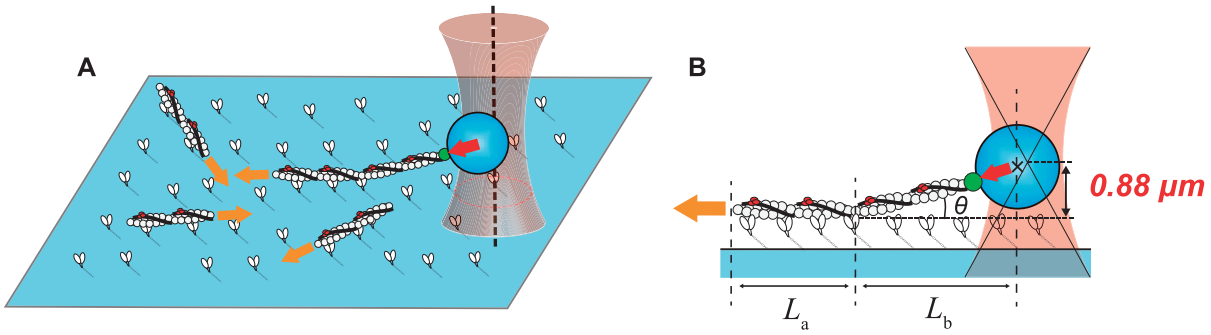

Figure 2 Method of measuring the sliding velocity and the angle-corrected sliding force using the *in vitro* motility assay system. (A) Reconstituted thin filaments that are either attached to a bead (1.0 μm in diameter) or freely sliding are illustrated. The filaments interact with HMM molecules that were immobilized on the surface of a glass cover-slip coated by collodion. The unloaded sliding velocity was measured by tracking the position of a thin filament freely moving without bead. The sliding force at the steady state was measured by trapping a bead-tailed thin filament by optical tweezers. The displacement of the bead from the trap center on the X–Y plane and the length of the thin filament interacting with myosin on the glass surface (L_a) were measured to determine the angle-corrected sliding force per unit length of the thin filament (F_{av}=F/length). (B) Due to the gap between the trap center (corresponding to the mass center of the trapped bead in the absence of sliding force) and the surface of the cover-slip (~0.88 μm [43]), the trapped bead is pulled towards the cover slip when active force is produced. From the predetermined gap size (0.88 μm) and the distance between the center of the bead and the end of the filament illuminated with TIRF system (L_b), the angle of force vector (θ) is geometrically estimated as θ=*arctan* (0.88 μm/L_b) [43].

were analyzed in each flow cell and the results were averaged. Seven to 48 filaments (N_{obs}; number of filaments or observation) and 400 to 2100 intervals were analyzed per each condition.

Measurement of the sliding force

The sliding force along the thin (or actin) filament was measured by using optical tweezers as described previously [43]. Typical time course of force measurement is shown in Supplementary Figure S1 (WT, pCa 5.0, L_a=3 μm). The cover slip surface was positioned at ~1 μm below a bead-tailed thin (or actin) filament trapped by the optical tweezers, where the focal plane of the florescence microscopy was located. The trap center was defined as the position of the trapped bead just before the actomyosin interaction takes place. The position of the bead was determined as the center of Gaussian distribution (analyzed by image J plugin; Particle Track and Analysis) that was fit to the 2D distribution of the pixel intensity of the bright-field image. The trap stiffness was set at 0.042–0.13 pN/nm which was controlled by the laser-power. Due to the gap between the trap center (bead) and the cover slip surface, the trapped bead was pulled vertically downwards in addition to horizontally upon sliding. Therefore, from the bead position in *X*-*Y* plane and the length of the filament illuminated by TIRF microscopy, the angle (θ) of the force vector was determined geometrically [43]. In this study, the angle-corrected force is represented as F. The F per unit length of the thin filament (F_{av}) was obtained by dividing F by the length of a part of the filament interacting with HMM (F_{av}=F/length). Seven to 16 force measurements were averaged per each condition.

Counting the number of cross-bridges formed under rigor condition

The number of cross-bridges was measured under the rigor condition as previously reported (Supplementary Fig. S2) [41,47]. The HMM-coated coverslip was prepared with HMM solution diluted to 5 μg/mL. Higher concentration was found to make the direct counting of rigor cross-bridges unreliable as the events of unbinding were indistinguishable from each other in our experimental condition.

The result was 1.35±0.15 heads/μm for 5 μg/mL HMM (N_{obs}=14 in 4 flow cells). The number of HMM molecules adsorbed to the coverslip surface was proportional to the HMM concentration [47,48]. Thus, the maximum number of available cross-bridges per unit length of the filament for 30 μg/mL HMM was estimated as 8.1 heads/μm, or rounded to 8 heads/μm in the subsequent description.

Analysis of the [Ca^{2+}] dependence

The dependence of sliding velocity (unloaded) or sliding force (at the steady state) on [Ca^{2+}] was analyzed. In the following equations, $Ca \equiv [Ca^{2+}]$ for simplicity.

$$v = v_{LC} + v_{act} H(Ca) \quad (1)$$

$$F_{av} = F_{LC} + F_{act} H(Ca) \quad (2)$$

where

$$H(Ca) \equiv \frac{1}{1+\left(\frac{Ca_{50}}{Ca}\right)^n} \quad (3)$$

Equation 3 is the Hill equation [16,34]. Ca_{50} is the apparent Ca^{2+} dissociation constant, and n is the Hill coefficient (constant) representing cooperativity of Ca^{2+} activation. pCa_{50} is

the pCa value at half saturation, which represents the Ca^{2+} sensitivity. In actuality, the constants of $H(Ca)$ in Eqs. 1–3 may be different in the case of velocity and force, so (v) or (f) is placed as a subscript, such as $Ca_{50(f)}$ and $n_{(f)}$. In the case of force, it was measured and averaged (F_{av}), and normalized using Eq. 4, which at the same time is $H(Ca)$ of Eq. 3:

$$H(Ca) \equiv \frac{F_{av} - F_{LC}}{F_{act}} \quad (4)$$

F_{LC} was deduced as the mean value of the force from the relaxing condition when pCa was in the range 8.0 and 9.0 (low [Ca^{2+}] or LC). F_{HC} was similarly deduced from the activating condition when pCa was in the range 4.0 and 5.8 (high [Ca^{2+}] or HC), where the force reached plateau. F_{act} is their difference ($F_{act} \equiv F_{HC} - F_{LC}$), which represents Ca^{2+}-activatable force. The results were fitted to Eq. 3 using Levenberg-Marquardt algorithm [49], which is a non-linear curve fitting program (KaleidaGraph, HULINKS). The normalization is for the purpose of good data fitting. A similar operation was repeated for the sliding velocity, v (Eqs. 1 through 4).

Statistical analysis

Experimental data was described as the mean±standard error of the mean (SEM). For paired comparisons, two-sided students' t-test was used. When the Pearson product-moment correlation coefficient (P) was calculated, the value t_{cal} was obtained from the degree of freedom M as $t_{cal} = P\sqrt{((M-2)/(1-P^2))}$ to obtain p-values using a Student's t-distribution.

Results

Ca^{2+} regulation of sliding velocity

To measure unloaded sliding velocity (v), non-bead-tailed thin filaments were used (Fig. 2A). The mean values of the sliding velocity between pCa 4.0 and 9.0 were plotted against pCa (Fig. 3A and 3B, all error bars were smaller than the symbol size, hence not seen). The pCa-velocity relationships were fitted to Eq. 4 to examine the difference between the thin filaments reconstituted with mutant Tpm and WT Tpm (Table 1). The sliding velocity at pCa ≥8 (v_{LC}) was significantly larger ($p<0.001$) in mutants than in WT (Fig. 3C). This incomplete relaxation may lead to a diastolic dysfunction, which is a characteristics of HCM [7]. The sliding velocity during activation (v_{HC}) was comparable between mutants and WT (Table 1). The Ca^{2+} activated velocity (v_{act}) was significantly less in mutants than in WT ($p<0.01$). These trends were also observed in our previous study using thin-filament reconstituted muscle fibers [16]. Both Ca^{2+} sensitivity ($pCa_{50(v)}$) and cooperativity ($n_{(v)}$) increased in mutants, but the increase was small and statistically insignificant (Table 1).

Ca^{2+} regulation of sliding force

To measure sliding force (F), bead-tailed thin filaments were used. Similar analysis to the velocity was performed on force, and force per unit thin-filament length ($F_{av}=F$/length) was plotted against pCa in Fig. 4 A and B. The force value was divided by the length, because it has long been known that force is proportional to the length [50]. The results were

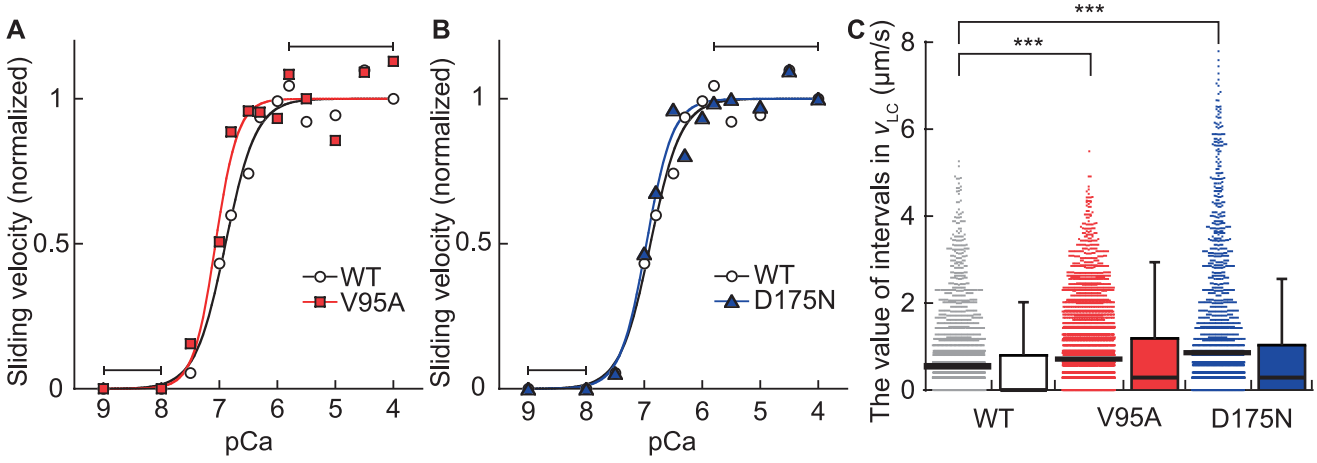

Figure 3 Ca^{2+}-dependence of the sliding velocity of the thin filaments reconstituted with Tpm mutants. (A and B) Sliding velocity at different pCa values was determined in *in vitro* motility assay for thin filaments reconstituted using WT Tpm (white circles) or Tpm mutants (V95A, red squares; D175N, blue triangles). Symbols and vertical error bars represent the mean±SEM (≥400 time intervals of 200 ms in each condition, based on ≥7 filaments, and 2 flow cells). Error bars are smaller than the symbol sizes and cannot be seen. Regression analysis was performed after the value of v_{LC} was subtracted from all the data and the resultant values were divided by v_{act}. Black, red and blue curves represent the best fit to Eq. 2 for WT, V95A and D175N, respectively. The best fit parameters and standard errors are shown in Table 1. The reconstituted thin filaments were relaxed between pCa 8.0 and 9.0 (horizontal bars), and fully activated between pCa 4.0 and 5.8 (horizontal bars). (C) Distribution of intervals in v_{LC} for WT and mutant Tpm in the range of pCa 8.0–9.0. Horizontal bars in dot plots represent average values. WT, v_{LC}=0.55±0.02 μm/s (mean±SEM, N_{obs}=15). V95A, 0.71±0.01 μm/s (N_{obs}=36). D175N, 0.86±0.03 μm/s (N_{obs}=21). *** $p<0.001$. In boxes and whisker plots, the horizontal thick lines represent the median value, and the top and bottom edges of boxes represent the first and third quartiles, respectively.

Table 1 Parameters for WT and Tpm mutants

Parameters	WT	V95A	D175N
v_{HC}, μm/s	7.16±0.02 (141)	6.98±0.02 (161)	7.39±0.02 (166)
v_{LC}, μm/s	0.55±0.02 (15)	0.71±0.01*** (36)	0.86±0.03*** (21)
v_{act}, μm/s	6.61±0.02 (141)	6.27±0.02***(161)	6.53±0.02** (166)
F_{HC}, pN/μm	2.95±0.15 (60)	2.39±0.10** (58)	3.54±0.12** (59)
F_{LC}, pN/μm	0.14±0.02 (21)	0.12±0.01 (21)	0.11±0.02 (19)
F_{act}, pN/μm	2.81±0.15 (60)	2.27±0.10** (58)	3.43±0.12** (59)
$n_{(v)}$	1.65±0.23	2.25±0.59	1.90±0.33
$pCa_{50(v)}$	6.89±0.04	7.07±0.06	6.96±0.04
$n_{(f)}$	1.50±0.46	1.13±0.35	2.11±0.51
$pCa_{50(f)}$	6.52±0.10	6.72±0.12	6.68±0.06
a, pN (stall force)	3.1	3.1	3.1
$\rho(a)$ (duty ratio)	0.118	0.096	0.143
$\rho(0)$	0.14±0.01	0.14±0.02	0.15±0.02
t_{on}, ms	0.75	0.77	0.73
t_{off}, ms	4.6	4.7	4.1

Comparable results on pure actin filaments were v=4.23±0.04 μm/s (N_{obs}=12), and F=2.37±0.15 pN/μm (N_{obs}=33). For algebraic averaged parameters, the mean±standard error of the mean (SEM) are shown together with the number of filaments or observations in ( ). For regression parameters, the best-fit value±standard error (SE) are shown. Two-sided students' t-test was used to describe statistical differences between a mutant and WT: * p<0.05; ** p<0.01; *** p<0.001.

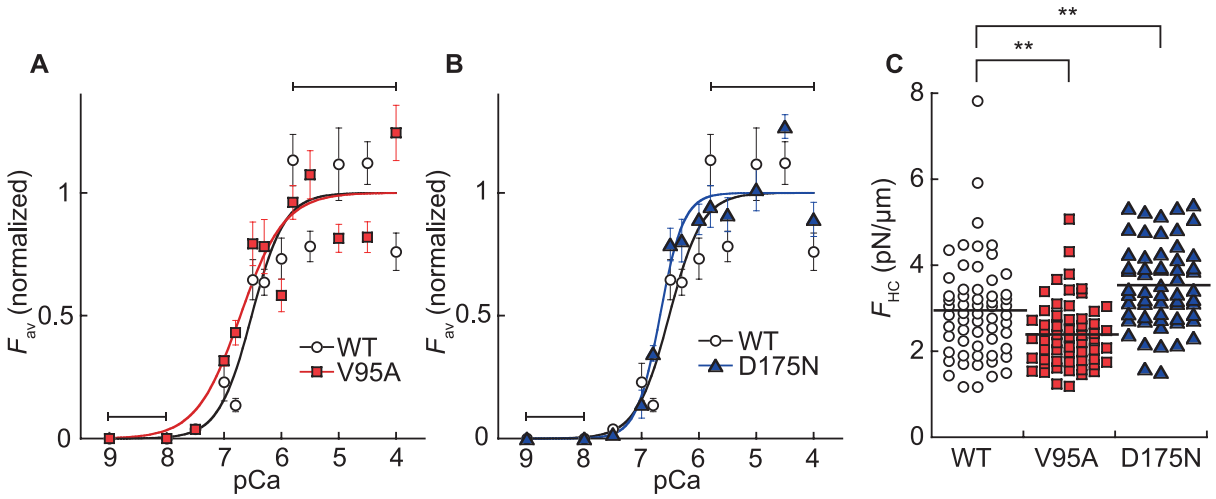

Figure 4 Ca^{2+}-dependence of the angle-corrected sliding force per unit length of thin filament. (A and B) The angle-corrected sliding force per unit length of the thin filament (F_{av}) at different pCa conditions were determined by using the *in vitro* motility assay with WT Tpm (white circles) and HCM Tpm mutants (V95A, red squares; D175N, blue triangles). Symbols and the vertical error bars represent the mean±SEM (≥7 measurements over 2 flow cells in each condition). Regression analysis was performed after the value of F_{LC} was subtracted from all the data points and the resuls were normalized to F_{act}. Black, red and blue curves represent the best fit curves to Eq. 3 for WT, V95A and D175N, respectively. Fitting parameters deduced are shown in Table 1. Solid horizontal bars at the top represent the fully activated condition (pCa 4.0–5.8), where the force is saturated. (C) Distribution of F_{HC} for WT and mutant Tpms in the range of pCa 4.0–5.8. Horizontal bars represent average values. WT, 2.95±0.15 pN/μm (mean±SEM, N_{obs}=60). V95A, 2.39±0.10 pN/μm (N_{obs}=58). D175N, 3.54±0.12 pN/μm (N_{obs}=59). Statistical analysis was performed as student's t-test. ** p<0.01.

fitted to Eq. 3 (solid lines in Fig. 4 A and B), and the regression parameters are listed in Table 1.

The maximum sliding force (F_{HC}) was 2.39±0.10 pN/μm (N_{obs}=58) in V95A, and 3.54±0.12 pN/μm (N_{obs}=59) in D175N, which were significantly different (p<0.01) from WT (2.95±0.15 pN/μm, N_{obs}=60) (Fig. 4C). As seen here, the two mutants exhibited opposite effects: F_{HC} was decreased in V95A but increased in D175N. The force values during relaxation (F_{LC}) were small, and not statistically different between mutants and WT (Table 1). This result may relate to the sensitivity of the measuring device (see Discussion).

The Ca^{2+} activated force ($F_{act}\equiv F_{HC}-F_{LC}$) decreased in V95A (2.27±0.10 pN/μm), and increased in D175N (3.43±0.12 pN/μm), both of which were significantly different (p<0.05) from that of WT (2.81±0.15 pN/μm). This effect is similar to F_{HC}. Both Ca^{2+} sensitivity ($pCa_{50(f)}$) and

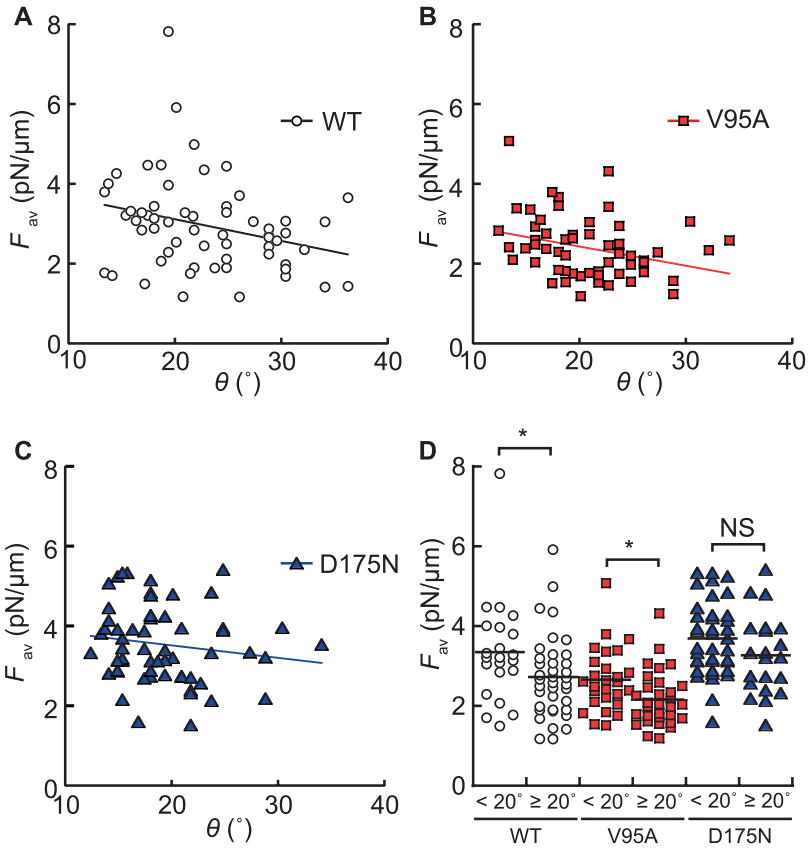

Figure 5 Correlation between active sliding force per unit length (F_{av}), and the angle of force vector. (A–C) Correlation between the angle-corrected sliding force per unit length of the thin filament (F_{av}=F/length) in the range of pCa 4.0–5.8, and the angle between the glass surface and the thin filaments (θ) reconstituted from WT (A, N_{obs}=60), V95A (B, N_{obs}=58), and D175N (C, 59 measurements) mutants of Tpm. Regression lines are (A) y=−0.054x+4.2, R=0.28; (B) y=−0.048x+3.4, R=0.30; and (C) y=−0.031x+4.1, R=0.15. (D) Distribution of F_{av} at θ<20° and θ≥20°. Data were statistically compared by using two-sided student's t-test (*p<0.05, NS= no significance).

Table 2 Angular dependence of sliding force F_{av}

	10°<θ≤20°	20°<θ<40°
WT	3.34±0.28 (22)	2.72±0.17* (38)
V95A	2.65±0.15 (27)	2.16±0.12* (31)
D175N	3.69±0.15 (38)	3.27±0.22 (21)

Average of the data in Fig. 5A–C. Units: pN/μm. * p<0.05 comparing below and above 20°. The number of thin filaments studied in ( ). The Pearson product-moment correlation coefficients for WT (P=−0.28, M=58; p<0.05), V95A (P=−0.30, M=56; p<0.05) and D175N (P=−0.15, M=57; p=0.25), where M is the degree of freedom. See Materials and Methods for details.

cooperativity ($n_{(f)}$) changed in mutants, but the change was small and statistically insignificant (Table 1).

Angular dependence of force

The angle of the force vector (θ) (Fig. 2B; [43]) was analyzed by plotting F_{av} against θ (Fig. 5A–C), and results are summarized in Table 2 and Figure 5D. F_{av} of θ above 20° was significantly less than that below 20° in WT, which was also the case in V95A. But there was no significant difference in D175N. The Pearson product-moment correlation coefficients for WT (P=−0.28, M=degree of freedom=58; p<0.05), V95A (P=−0.30, M=56; p<0.05), and D175N (P=−0.15, M=57; p=0.25) demonstrate this point.

Duty ratio of cross-bridges

We have deduced the duty ratio at the steady state of force in the saturating [Ca^{2+}] (Supplementary Fig. S1) and unloaded condition. To account for the difference in sliding force, we adopted the model developed to describe sliding force per unit length of the thin filament [51].

Stall force (a) for single myosin molecule is given as

$$a = dK_{cb} = 5.4\,\text{nm} \times 0.58\,\text{pNnm}^{-1} = 3.1\,\text{pN} \quad (5)$$

where d is step size (5.4 nm) measured when trap stiffness was 0.1 pN/nm and K_{cb} is cross-bridge stiffness (0.58 pN/nm) [52,53]. d and K_{cb} are thought to reflect the characteristics of myosin molecules and not affected by Tpm mutants. Consequently, the same a is used for mutants and WT (Table 1).

However, these values varied among previous reports: much higher stiffness values were obtained from single molecule or single fiber measurements, and they were

1–3 pN/nm [54–57]; the random orientation of myosin heads may affect the force per cross-bridge [58,59]. Therefore, the estimate of a includes an ambiguity and lack of consideration of elasticity of myosin heads [57]. The value of a (3.1 pN) is not in conflict with a previous report that focused on motor coupling coordination [60]; the values of d and K_{cb} were obtained with essentially the same experimental setup as used in the current study.

The sliding force at saturating Ca^{2+} (F_{HC}) is the product of the maximum number of available cross-bridges (N_{max}), the stall force for the cross-bridge (a), and the duty ratio ($\rho(a)$):

$$F_{HC} = N_{max}\, a\rho(a) \tag{6}$$

where N_{max} is estimated to be 8 heads/μm in the current study (cf. *Materials and Methods*). $\rho(a)$ is determined as:

$$\rho(a) = F_{HC}/(N_{max}\, a) = F_{HC}/(8 \text{ heads/μm} \times 3.1 \text{ pN}) \tag{7}$$

from Eq. 6. The values of $\rho(a)$ are calculated from F_{HC} in Table 1 and resulted in 0.118, 0.096, and 0.143, for WT, V95A, and D175N, respectively (Table 1). These are different in mutants from WT, because F_{HC} values are different. While an ambiguity in a leads to an ambiguity in $\rho(a)$, the main purpose of this estimate is a comparison, and not their absolute values.

The Ca^{2+} dependence of the time averaged force is:

$$F_{av} = F_{HC}\, H(Ca) \tag{8}$$

Therefore, from Eq. 6

$$F_{av} = N_{max}\, a\rho(a)\, H(Ca) \tag{9}$$

The formalism of Eq. 6 was developed by Stam *et al*. [50]. As shown in Eq. 6, F_{av} is proportional to the duty ratio $\rho(a)$, as assumed previously [19,51,61].

We then examined the duty ratio $\rho(0)$ at the unloaded condition. Uyeda *et al.* described Ca^{2+}-dependence of the sliding velocity (v) as a function of the number of force-generating cross-bridges [45];

$$v = v_0\{1 - (1 - \rho(0))^N\} \tag{10}$$

where v_0 is the maximum sliding velocity, and N is the number of force-generating cross-bridges per thin filament that changes with pCa. $v_0 = d/t_{on}$, where t_{on} is the duration during which the cross-bridge is attached [45,62]. In the current study, $v_0 = v_{HC}$. Because 2–4 μm long filaments were analyzed in the current study, the maximum number of cross-bridges per thin filament is $N = 8$ heads/μm × 3 μm = 24 heads (cross-bridges), where 3 μm is the median filament length. Longyear *et al.* suggested that Tpm and Tn regulate the event frequency of cross-bridge formation by Ca^{2+}-dependent manner [63]. The only parameter that is Ca^{2+}-dependent in Eq. 9 is $H(Ca)$, which is defined as the indicator of the event frequency. Homsher *et al.* suggested that the relative force obtained as per unit length of the filament, F_{av}/F_{HC} can be considered as a fraction of the number of force generating cross-bridges [64]. Consequently, the Ca^{2+}-dependent event frequency of cross-bridge formation (N) is estimated to be $24\,H(Ca)$, obtained from parameters for sliding force. The data of pCa-dependent sliding velocity (Fig. 3) is replotted as a function of $24H$ (Fig. 6), and analyzed using Eq. 10 to deduce $\rho(0)$ by regression. $\rho(0)$ of mutants is not significantly different from that of WT (Table 1).

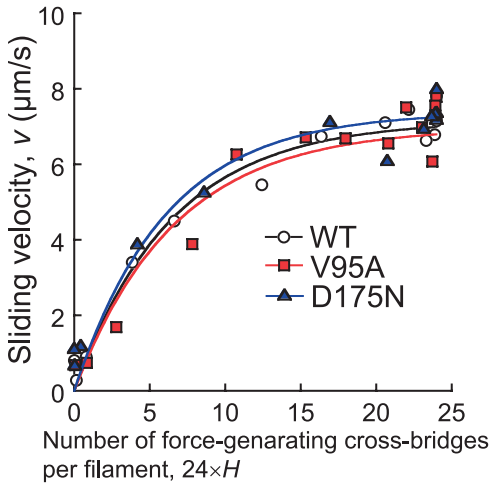

Figure 6 $H(Ca)$ function and the dependence of sliding velocity on the number of cross-bridges. pCa-dependence of the sliding velocity (v) (Fig. 1) was reevaluated by using the $H(Ca)$ function, which also depends on pCa_{50} (Ca^{2+} sensitivity) and n (cooperativity), to estimate the number of force-generating cross-bridges (8 heads/μm × 3 μm × $H(Ca)$ = 24 × $H(Ca)$). The data of sliding velocity vs. pCa are replotted as functions of force-generating cross-bridges (WT: open circles, V95A: red squares, D175N: blue triangles), and regression analysis was performed to estimate duty ratio at unloaded condition. Black, red and blue curves represent the best fit to WT, V95A and D175N, respectively (Eq. 10).

Molecular friction

It would be interesting to examine coupling between the sliding velocity and the force among different mutants. Their direct coupling has been proposed by Sato *et al.* [65], and shown by our previous study [32]. These investigations demonstrated that the sliding velocity is proportionally related to the sliding force in the thin filaments reconstituted with WT Tpm when the density of myosin molecule was kept constant [32]. Sato *et al.* proposed that the proportional relationship exists between unloaded sliding velocity and active cross-bridge force generated.

Figure 7 summarizes the relationship between the sliding velocity (v_{HC}) and the force ($F_{av} = F_{HC}$), listed in Table 1. As seen in this figure, the molecular friction (reciprocal slope of Fig. 7) is similar between pure actin filaments and D175N, less in WT, and least in V95A. The measurements with pure actin filaments were $v_{HC} = 4.23 \pm 0.04$ μm/s ($N_{obs} = 12$),

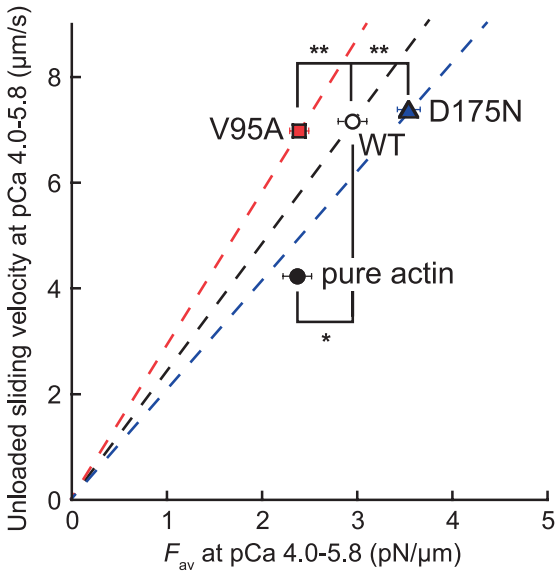

Figure 7 Modulated molecular friction by Tpm mutants. To evaluate the molecular friction due to cross-bridges, unloaded sliding velocity was plotted against the sliding force per unit length of filament, F_{av}. The reciprocal of the slope for the linear relationship represents the molecular friction. See text for details. The unloaded sliding velocities and the sliding forces of WT, V95A, and D175N are the averages at pCa 4.0–5.8. The data for pure actin filaments were obtained at pCa 5 (Black circles). Statistical analysis was performed as student's *t*-test. * $p<0.05$, ** $p<0.01$. Symbols and error bars represent the mean±SEM.

and F_{HC}=2.37±0.15 pN/μm (N_{obs}=33). In the presence of WT Tpm/Tn, v_{HC} ($p<0.001$) and F_{HC} ($p<0.05$) were enhanced as previously reported [32].

Discussion

Contractile dysfunctions and their molecular bases

Diastolic dysfunction (incomplete relaxation) is characteristic of HCM [7]. In fact, we observed increased sliding velocity (v_{LC}) at the relaxing condition (pCa≥8.0) in both mutants (Table 1). Comparable results were obtained in the thin filament-reconstituted cardiac muscle fibers with Tpm mutants V95A, D175N, and E180G [16]. Similar increase was not detected in F_{LC}, presumably because our detection system was not sensitive enough to the very low force level. Two groups reported contrary results using *in vitro* motility assay [22,34]. This difference may be based on lower ionic strength used in the present study. Low ionic strength increases electrostatic interaction between actin and Tpm, and modulates actin and myosin interaction.

In V95A, v_{act}, F_{act}, and F_{HC} decreased (Table 1), which presumably stem from the same mechanisms and cause less ejection fraction, resulting in less blood pumped during systole. Both of these problems can lead into HCM. In D175N, F_{act} and F_{HC} increased (Table 1), which is a gain of function and may not cause an immediate systolic problem, but the incomplete relaxation may still cause a diastolic problem to result in HCM. Increased Ca^{2+} sensitivity has been considered a hallmark of HCM [21,22,34]. While our results show small increases in pCa_{50}, but their increases are not statistically significant both in velocity and force in either mutant (Table 1), hence our results do not support this hypothesis. The change in pCa_{50} depends on experimental conditions, such as ionic strength, [ATP], and [Pi] [16], and the experimental method may be an additional factor. Furthermore, the effect is sometimes opposite, hence a change in pCa_{50} may not be the direct cause of HCM [25].

A limitation of our results may be the use of skeletal myosin rather than cardiac myosin. The reported difference between skeletal and cardiac myosin is the ATPase turnover rate [66] and the nucleotide affinity [67–71]. In contrast it was reported that Ca^{2+} sensitivity does not depend on myosin isoforms [33,35] under the saturated ATP concentration in the virtual absence of ADP. Because our study is focused on the functional effects of mutations in Tpm, the observed relative changes caused by mutants seem to be sufficiently meaningful.

The v_{HC} is similar (proportional) to d/t_{on}. Shchepkin *et al.* demonstrated previously that the step size (d) is not any different in Tpm mutants they have tested [72]. Although V95A and D175N were not included in their study, there is no reason to believe that d (therefore, t_{on} as well) is affected by these mutants.

The duty ratio at the unloaded condition, $\rho(0)=t_{on}/[t_{on}+t_{off}]$ (t_{off} is detached duration) is comparable in mutants and WT (Table 1). This is consistent with a previous report by Wang *et al.* [34], where D175N had no effect on the duty ratio. Because t_{on} is not affected by the mutants, this result suggests that t_{off} is not affected by mutants.

The opposite effects of both mutants on sliding force (F_{HC}) must be related to the duty ratio at the steady state, $\rho(a)$. In our analysis, $\rho(a)$ is smaller by 19% in V95A than WT, whereas it is larger by 21% in D175N than WT. The smaller active force in V95A, in which hydrophobicity changes without changing the electrical charge, is consistent with the results obtained in our previous study using reconstituted muscle fibers [16]. Although the values of $\rho(0)$ for WT and D175N were comparable (Table 1), $\rho(a)$ for D175N was substantially larger than that for WT. This result suggests that D175N may affect the load-dependence of cross-bridge formation.

Furthermore, we have observed that D175N maintains the sliding force more stable than WT when the thin filament was pulled vertically by optical tweezers (Fig. 5). These modulations by D175N must stem from a charge change from Asp (−1) to Asn (0) that modifies electrostatic interaction between actin and Tpm, and/or actin and myosin via Tpm.

Advantages using the *in vitro* motility assay

The *in vitro* motility assay as used in the current study could highlight the effect of the ionic strength on the force

generation than other assay systems. The increased active force for D175N is at variance from previous studies that the active force for D175N was not different from that of WT in muscles from transgenic mouse models in which mutant Tpm was expressed [73], and in an *in vitro* motility assay in the presence of α-actinin as drag force to immobilize thin filaments on coverslip [21]. Furthermore, smaller active force was reported in reconstituted muscle fibers using D175N than WT [16]. Optical tweezers assay used in the present study measures the sliding force directly, enhancing the difference between D175N and WT. The difference observed in muscle fibers may be caused by the difference in ionic strength. The current study used 50 mM, whereas fiber studies used 200 mM, which is physiological but makes less sensitive to the ionic interaction. The change in the surface charge in D175N of Tpm is expected to stabilize the force generation process at lower ionic strength because ionic atmosphere is larger in lower ionic strength [74] as in the current study.

In transgenic animal models, expression of a Tpm mutant cannot achieve the 100% level, and the mutant Tpm coexists with WT Tpm. Such a heterogeneous expression may cause additional effects on contractility due to mismatching at the head-to-tail association between adjacent Tpm molecules [75–77]. These experimental differences may underlie the differences in the results.

Conclusion

We studied a functional significance of HCM mutants of Tpm, V95A and D175N, using *in vitro* motility assays. A failure of inhibition of sliding motion (v_{LC}) at low [Ca^{2+}] in both mutants may induce diastolic dysfunction that has been thought to be the major cause of the pathogenesis of Tpm-associated HCM. The changes in sliding force (F_{HC}) in V95A (decrease) and D175N (increase) were in two different directions, possibly because two mutants modulate the molecular process of actomyosin interaction differently. These results suggest that the *in vitro* motility assay is sensitive to the ionic interaction including actin-Tpm interaction, and is able to distinguish the property of HCM mutants of Tpm based on sliding force and velocity.

Acknowledgement

We thank Prof. P. B. Chase (Florida State University) and Dr. Aya K. Takeda (Florida State University) for providing α-Tropomyosin (Tpm) WT, Dr. M. Miyazaki (Waseda University) for providing a custom-built software to interface a camera and a computer, Dr. Y. Arai (Osaka University) for ImageJ plugin software, Prof. K. Yasuda and his members (Waseda University) for valuable advice and discussions. This work was supported by grants from the US National Institutes of Health HL070041 and US American Heart Association 13GRNT16810043 (to MK), JSPS KAKENHI Grant Number 22227005 (to S. Ishiwata), and by The Japan Science and Technology Agency Grant Number JPMJPR15F5 (to MS). The content is solely the responsibility of the authors and does not necessarily reflect the official views of the funding organizations.

Conflict of Interest

The authors declare no conflict of interest.

Author Contribution

S. I., M. S., S. I., and M. K. designed the experiments. S. I. and M. K. parepared proteins. S. I. acquired and analyzed the data. S. I., M. S., S. I. and M. K. wrote the manuscript. All authors discussed the contents and approved the manuscript.

Symbols and Abbreviations Used

- a Stall force for single myosin molecule, $a = dK_{cb} = 5.4\ \text{nm} \times 0.58\ \text{pN/nm} = 3.1\ \text{pN}$
- Ca ≡ [Ca^{2+}] Free Ca^{2+} concentration
- Ca_{50} Apparent Ca^{2+} dissociation constant. [Ca^{2+}] of half saturation.
- d Step size (measured when the trap stiffness is 0.1 pN/nm), $d = 5.4$ nm
- F Sliding force of a filament. All F values (below) are angle corrected [43]
- F_{act} Ca^{2+}-activatable sliding force/unit length, $F_{act} = F_{HC} - F_{LC}$
- F_{av} Time averaged sliding force/unit length, $F_{av} = F$/length
- F_{HC} Sliding force/unit length in saturating [Ca^{2+}], $F_{HC} \equiv F_{LC} + F_{act} = 8\, a\rho(a)$
- F_{LC} Sliding force/unit length in the absence of Ca^{2+}
- fps Frames/s
- $H(Ca) \equiv \dfrac{1}{1+\left(\dfrac{Ca_{50}}{Ca}\right)^n}$ H is also a function of Ca_{50} and n
- HC High Ca (pCa 4.0–5.8)
- K_{cb} Cross-bridge stiffness, $K_{cb} = 0.58$ pN/nm
- L_a The length of the thin filament interacting with myosin
- L_b The distance between the center of the bead and the end of the filament
- LC Low Ca (pCa 8.0–9.0)
- M Degree of freedom
- n Hill coefficient. (v) is placed to indicate based on unloaded sliding velocity, and (f) to indicate sliding force measurements
- N Number of force-generating cross-bridges per thin filament (Ca dependent), $N = 24H$, when the filament length is 3 μm and the head density is 8 heads/μm.
- N_{max} The maximum number of available cross-bridges per unit length of thin filament, $N_{max} = 8$ head/μm

N_{obs} Number of observations; number of filaments
P Pearson product-moment correlation coefficient
pCa $\equiv -\log [Ca^{2+}]$
pCa_{50} $\equiv -\log Ca_{50}$: Ca^{2+} sensitivity. (v) is placed to indicate based on unloaded sliding velocity, and (f) to indicate sliding force measurements
$\rho(0)$ Duty ratio at the unloaded condition
$\rho(a)$ Duty ratio determined at the steady state of force generation in saturating $[Ca^{2+}]$
t_{cal} t-value calculated for Pearson product-moment correlation coefficient.
t_{off} Detached duration at saturating $[Ca^{2+}]$
t_{on} Attached duration at saturating $[Ca^{2+}]$
θ The angle of the sliding force vector out of the X-Y plane
v Unloaded sliding velocity of filaments
v_0 The maximum sliding velocity, $v_0=d/t_{on}$, v_0 corresponds to v_{HC} in the current study
v_{act} Ca^{2+}-activatable sliding velocity, $v_{act}=v_{HC}-v_{LC}$
v_{HC} Sliding velocity in saturating $[Ca^{2+}]$, $v_{HC}=v_{LC}+v_{act}$
v_{LC} Sliding velocity in the absence of Ca^{2+}

References

[1] Spirito, P., Seidman, C., McKenna, W. & Maron, B. J. The Management of hypertrophic cardiomyopathy. *N. Engl. J. Med.* **336**, 775–785 (1997).
[2] Maron, B. J., McKenna, W. J., Danielson, G. K., Kappenberger, L. J., Kuhn, H. J., Seidman, C. E., *et al.* American college of cardiology/european society of cardiology clinical expert consensus document on hypertrophic cardiomyopathy. *J. Am. Coll. Cardiol.* **42**, 1687–1713 (2003).
[3] Elliott, P. & McKenna, W. J. Hypertrophic cardiomyopathy. *Lancet* **363**, 1881–1891 (2004).
[4] Ho, C. Y. & Seidman, C. E. A contemporary approach to hypertrophic cardiomyopathy. *Circulation* **113**, 858–862 (2006).
[5] Poliac, L. C., Barron, M. E. & Maron, B. J. Hypertrophic cardiomyopathy. *Anesthesiology* **104**, 183–192 (2006).
[6] Marston, S. B. How do mutations in contractile proteins cause the primary familial cardiomyopathies? *J. Cardiovasc. Transl. Res.* **4**, 245–255 (2011).
[7] Redwood, C. & Robinson, P. Alpha-tropomyosin mutations in inherited cardiomyopathies. *J. Muscle Res. Cell Motil.* **34**, 285–294 (2013).
[8] Marsiglia, J. D. C. & Pereira, A. C. Hypertrophic cardiomyopathy: how do mutations lead to disease? *Arq. Bras. Cardiol.* **102**, 295–304 (2014).
[9] Ommen, S. R. & Gersh, B. J. Sudden cardiac death risk in hypertrophic cardiomyopathy. *Eur. Heart J.* **30**, 2558–2559 (2009).
[10] Marian, A. J. & Roberts, R. The molecular genetic basis for hypertrophic cardiomyopathy. *J. Mol. Cell. Cardiol.* **33**, 655–670 (2001).
[11] Barron, J. T. Hypertrophic cardiomyopathy. *Curr. Treat. Options Cardiovasc. Med.* **1**, 277–282 (1999).
[12] Kawai, M. & Ishiwata, S. Use of thin filament reconstituted muscle fibres to probe the mechanism of force generation. *J. Muscle Res. Cell Motil.* **27**, 455–468 (2006).
[13] Terui, T., Sodnomtseren, M., Matsuba, D., Udaka, J., Ishiwata, S., Ohtsuki, I., *et al*. Troponin and titin coordinately regulate length-dependent activation in skinned porcine ventricular muscle. *J. Gen. Physiol.* **131**, 275–283 (2008).
[14] McLeod, C. J., Bos, J. M., Theis, J. L., Edwards, W. D., Gersh, B. J., Ommen, S. R., *et al*. Histologic characterization of hypertrophic cardiomyopathy with and without myofilament mutations. *Am. Heart J.* **158**, 799–805 (2009).
[15] Marian, A. J. Pathogenesis of diverse clinical and pathological phenotypes in hypertrophic cardiomyopathy. *Lancet* **355**, 58–60 (2000).
[16] Bai, F., Weis, A., Takeda, A. K., Chase, P. B. & Kawai, M. Enhanced active cross-bridges during diastole: molecular pathogenesis of tropomyosin's HCM mutations. *Biophys. J.* **100**, 1014–1023 (2011).
[17] Marian, A. J., Yu, Q. T., Mann, D. L., Graham, F. L. & Roberts, R. Expression of a mutation causing hypertrophic cardiomyopathy disrupts sarcomere assembly in adult feline cardiac myocytes. *Circ. Res.* **77**, 98–106 (1995).
[18] Yang, Q., Sanbe, A., Osinska, H., Hewett, T. E., Klevitsky, R. & Robbins, J. A mouse model of myosin binding protein C human familial hypertrophic cardiomyopathy. *J. Clin. Invest.* **102**, 1292–1300 (1998).
[19] Tyska, M. J., Hayes, E., Giewat, M., Seidman, C. E., Seidman, J. G. & Warshaw, D. M. Single-molecule mechanics of R403Q cardiac myosin isolated from the mouse model of familial hypertrophic cardiomyopathy. *Circ. Res.* **86**, 737–744 (2000).
[20] Bottinelli, R., Coviello, D. A., Redwood, C. S., Pellegrino, M. A., Maron, B. J., Spirito, P., *et al*. A mutant tropomyosin that causes hypertrophic cardiomyopathy is expressed in vivo and associated with an increased calcium sensitivity. *Circ. Res.* **82**, 106–115 (1998).
[21] Bing, W., Knott, A., Redwood, C., Esposito, G., Purcell, I., Watkins, H., *et al*. Effect of hypertrophic cardiomyopathy mutations in human cardiac muscle alpha-tropomyosin (Asp175Asn and Glu180Gly) on the regulatory properties of human cardiac troponin determined by *in vitro* motility assay. *J. Mol. Cell. Cardiol.* **32**, 1489–1498 (2000).
[22] Karibe, A., Tobacman, L. S., Strand, J., Butters, C., Back, N., Bachinski, L. L., *et al*. Hypertrophic cardiomyopathy caused by a novel alpha-tropomyosin mutation (V95A) is associated with mild cardiac phenotype, abnormal calcium binding to troponin, abnormal myosin cycling, and poor prognosis. *Circulation* **103**, 65–71 (2001).
[23] Chang, A. N., Harada, K., Ackerman, M. J. & Potter, J. D. Functional consequences of hypertrophic and dilated cardiomyopathy-causing mutations in alpha-tropomyosin. *J. Biol. Chem.* **280**, 34343–34349 (2005).
[24] Ly, S. & Lehrer, S. S. Long-range effects of familial hypertrophic cardiomyopathy mutations E180G and D175N on the properties of tropomyosin. *Biochemistry* **51**, 6413–6420 (2012).
[25] Bai, F., Wang, L. & Kawai, M. A study of tropomyosin's role in cardiac function and disease using thin-filament reconstituted myocardium. *J. Muscle Res. Cell Motil.* **34**, 295–310 (2013).
[26] Kim, S. J., Iizuka, K., Kelly, R. A., Geng, Y. J., Bishop, S. P., Yang, G., *et al*. An alpha-cardiac myosin heavy chain gene mutation impairs contraction and relaxation function of cardiac myocytes. *Am. J. Physiol*. **276**, H1780–H1787 (1999).
[27] McLachlan, A. D. & Stewart, M. Tropomyosin coiled-coil interactions: Evidence for an unstaggered structure. *J. Mol. Biol.* **98**, 293–304 (1975).
[28] Hitchcock-DeGregori, S. E., Song, Y. & Greenfield, N. J. Functions of tropomyosin's periodic repeats. *Biochemistry* **41**, 15036–15044 (2002).
[29] Lu, X., Tobacman, L. S. & Kawai, M. Effects of tropomyosin internal deletion Δ23Tm on isometric tension and the cross-bridge kinetics in bovine myocardium. *J. Physiol.* **553**, 457–471 (2003).

[30] Lu, X., Tobacman, L. S. & Kawai, M. Temperature-dependence of isometric tension and cross-bridge kinetics of cardiac muscle fibers reconstituted with a tropomyosin internal deletion mutant. *Biophys. J.* **91**, 4230–4240 (2006).
[31] Kawai, M., Lu, X., Hitchcock-DeGregori, S. E., Stanton, K. J. & Wandling, M. W. Tropomyosin period 3 is essential for enhancement of isometric tension in thin filament-reconstituted bovine myocardium. *J. Biophys.* **2009**, 1–17 (2009).
[32] Oguchi, Y., Ishizuka, J., Hitchcock-DeGregori, S. E., Ishiwata, S. & Kawai, M. The role of tropomyosin domains in cooperative activation of the actin-myosin interaction. *J. Mol. Biol.* **414**, 667–680 (2011).
[33] Schoffstall, B., Brunet, N. M., Williams, S., Miller, V. F., Barnes, A. T., Wang, F., *et al*. Ca^{2+} sensitivity of regulated cardiac thin filament sliding does not depend on myosin isoform. *J. Physiol*. **577**, 935–944 (2006).
[34] Wang, F., Brunet, N. M., Grubich, J. R., Bienkiewicz, E. A., Asbury, T. M., Compton, L. A., *et al*. Facilitated cross-bridge interactions with thin filaments by familial hypertrophic cardiomyopathy mutations in α-tropomyosin. *J. Biomed. Biotechnol.* **2011**, 1–12 (2011).
[35] Fujita, H., Yasuda, K., Niitsu, S., Funatsu, T. & Ishiwata, S. Structural and functional reconstitution of thin filaments in the contractile apparatus of cardiac muscle. *Biophys. J.* **71**, 2307–2318 (1996).
[36] Suzuki, N., Miyata, H., Ishiwata, S. & Kinosita Jr., K. Preparation of bead-tailed actin filaments: estimation of the torque produced by the sliding force in an *in vitro* motility assay. *Biophys. J.* **70**, 401–408 (1996).
[37] Potter, J. D. Preparation of troponin and its subunits. *Methods Enzymol.* **85**, 241–263 (1982).
[38] Kurokawa, H., Fujii, W., Ohmi, K., Sakurai, T. & Nonomura, Y. Simple and rapid purification of brevin. *Biochem. Biophys. Res. Commun.* **168**, 451–457 (1990).
[39] Suzuki, M., Fujita, H. & Ishiwata, S. A new muscle contractile system composed of a thick filament lattice and a single actin filament. *Biophys. J.* **89**, 321–328 (2005).
[40] Suzuki, M. & Ishiwata, S. Quasiperiodic distribution of rigor cross-bridges along a reconstituted thin filament in a skeletal myofibril. *Biophys. J.* **101**, 2740–2748 (2011).
[41] Kawai, M., Kido, T., Vogel, M., Fink, R. H. A. & Ishiwata, S. Temperature change does not affect force between regulated actin filaments and heavy meromyosin in single-molecule experiments. *J. Physiol.* **574**, 877–887 (2006).
[42] Ishiwata, S. A study on the F-actin-tropomyosin-troponin complex: I. Gel-filament transformation. *Biochim. Biophys. Acta* **303**, 77–89 (1973).
[43] Ishii, S., Kawai, M., Ishiwata, S. & Suzuki, M. Estimation of actomyosin active force maintained by tropomyosin and troponin complex under vertical forces in the in vitro motility assay system. *PLoS ONE* **13**, 1–16 (2018).
[44] Gordon, A. M., Lamadrid, M. A., Chen, Y., Luo, Z. & Chase, P. B. Calcium regulation of skeletal muscle thin filament motility in vitro. *Biophys. J.* **72**, 1295–1307 (1997).
[45] Uyeda, T. Q. P., Kron, S. J. & Spudich, J. A. Myosin step size estimation from slow sliding movement of actin over low densities of heavy meromyosin. *J. Mol. Biol.* **214**, 699–710 (1990).
[46] Hilbert, L., Bates, G., Roman, H. N., Blumenthal, J. L., Zitouni, N. B., Sobieszek, A., *et al*. Molecular mechanical differences between isoforms of contractile actin in the presence of isoforms of smooth muscle tropomyosin. *PLoS Comput. Biol.* **9**, 1–9 (2013).
[47] Nishizaka, T., Seo, R., Tadakuma, H., Kinosita, K. & Ishiwata, S. Characterization of single actomyosin rigor bonds: load dependence of lifetime and mechanical properties. *Biophys. J.* **79**, 962–974 (2000).
[48] Guo, B. & Guilford, W. H. The tail of myosin reduces actin filament velocity in the in vitro motility assay. *Cell Motil. Cytoskeleton* **59**, 264–272 (2004).
[49] Gavin, H. The Levenberg-Marquardt Method for Nonlinear Least Squares Curve-Fitting Problems. *Duke University*, 1–15 (2016) https://www.semanticscholar.org/paper/The-Levenberg-Marquardt-method-for-nonlinear-least-Gavin/1829418bae60a0b9f6efa38005b9f527be6e9570 (Last access January 21, 2019)
[50] Kishino, A. & Yanagida, T. Force measurements by micromanipulation of a single actin filament by glass needles. *Nature* **334**, 74–76 (1988).
[51] Stam, S., Alberts, J., Gardel, M. L. & Munro, E. Isoforms confer characteristic force generation and mechanosensation by myosin II filaments. *Biophys. J.* **108**, 1997–2006 (2015).
[52] Miyata, H., Yoshikawa, H., Hakozaki, H., Suzuki, N., Furuno, T., Ikegami, A., *et al*. Mechanical measurements of single actomyosin motor force. *Biophys. J.* **68**, 286s–290s (1995).
[53] Nishizaka, T., Miyata, H., Yoshikawa, H., Ishiwata, S. & Kinosita Jr., K. Unbinding force of a single motor molecule of muscle measured using optical tweezers. *Nature* **377**, 251–254 (1995).
[54] Linari, M., Caremani, M., Piperio, C., Brandt, P. & Lombardi, V. Stiffness and fraction of myosin motors responsible for active force in permeabilized muscle fibers from rabbit psoas. *Biophys. J.* **92**, 2476–2490 (2007).
[55] Piazzesi, G., Reconditi, M., Linari, M., Lucii, L., Bianco, P., Brunello, E., *et al*. Skeletal muscle performance determined by modulation of number of myosin motors rather than motor force or stroke size. *Cell* **131**, 784–795 (2007).
[56] Adamovic, I., Mijailovich, S. M. & Karplus, M. The elastic properties of the structurally characterized myosin II S2 subdomain: A molecular dynamics and normal mode analysis. *Biophys. J.* **94**, 3779–3789 (2008).
[57] Kaya, M. & Higuchi, H. Nonlinear elasticity and an 8-nm working stroke of single myosin molecules in myofilaments. *Science* **329**, 686–689 (2010).
[58] Tanaka, H., Ishijima, A., Honda, M., Saito, K. & Yanagida, T. Orientation dependence of displacements by a single one-headed myosin relative to the actin filament. *Biophys. J.* **75**, 1886–1894 (1998).
[59] Pertici, I., Bongini, L., Melli, L., Bianchi, G., Salvi, L., Falorsi, G., *et al*. A myosin II nanomachine mimicking the striated muscle. *Nat. Commun.* **9**, 1–10 (2018).
[60] Kaya, M., Tani, Y., Washio, T., Hisada, T. & Higuchi, H. Coordinated force generation of skeletal myosins in myofilaments through motor coupling. *Nat. Commun.* **8**, 1–13 (2017).
[61] Rao, V. S., Marongelli, E. N. & Guilford, W. H. Phosphorylation of tropomyosin extends cooperative binding of myosin beyond a single regulatory unit. *Cell Motil. Cytoskeleton* **66**, 10–23 (2009).
[62] Harada, Y., Sakurada, K., Aoki, T., Thomas, D. D. & Yanagida, T. Mechanochemical coupling in actomyosin energy transduction studied by in vitro movement assay. *J. Mol. Biol.* **216**, 49–68 (1990).
[63] Longyear, T., Walcott, S. & Debold, E. P. The molecular basis of thin filament activation: from single molecule to muscle. *Sci. Rep.* **7**, 1–12 (2017).
[64] Homsher, E., Lee, D. M., Morris, C., Pavlov, D. & Tobacman, L. S. Regulation of force and unloaded sliding speed in single thin filaments: effects of regulatory proteins and calcium. *J. Physiol.* **524**, 233–243 (2000).
[65] Sato, K., Ohtaki, M., Shimamoto, Y. & Ishiwata, S. A theory on auto-oscillation and contraction in striated muscle. *Prog. Biophys. Mol. Biol.* **105**, 199–207 (2011).

[66] Mijailovich, S. M., Nedic, D., Svicevic, M., Stojanovic, B., Walklate, J., Ujfalusi, Z., *et al.* Modeling the actin.myosin ATPase cross-bridge cycle for skeletal and cardiac muscle myosin isoforms. *Biophys. J.* **112**, 984–996 (2017).
[67] Shimizu, H., Fujita, T. & Ishiwata, S. Regulation of tension development by MgADP and Pi without Ca^{2+}; Role in spontaneous tension oscillation of skeletal muscle. *Biophys. J.* **61**, 1087–1098 (1992).
[68] Ishiwata, S. & Yasuda, K. Mechano-chemical coupling in spontaneous oscillatory contraction of muscle. *Phase Transitions*, **45**, 105–136 (1993).
[69] Yamashita, H., Sata, M., Sugiura, S., Momomura, S., Serizawa, T. & lizuka, M. ADP inhibits the sliding velocity of fluorescent actin filaments on cardiac and skeletal myosins. *Circ. Res.* **74**, 1027–1033 (1994).
[70] Fukuda, N., Fujita, H., Fujita, T. & Ishiwata, S. Regulatory roles of MgADP and calcium in tension development of skinned cardiac muscle. *J. Muscle Res. Cell Motil.* **19**, 909–921 (1998).
[71] Fukuda, N., Kajiwara, H., Ishiwata, S. & Kurihara, S. Effects of MgADP on length dependence of tension generation in skinned rat cardiac muscle. *Circ. Res.* **86**, 1–6 (2000).
[72] Shchepkin, D. V., Nabiev, S. R., Kopylova, G. V., Matyushenko, A. M., Levitsky, D. I., Bershitsky, S. Y., *et al*. Cooperativity of myosin interaction with thin filaments is enhanced by stabilizing substitutions in tropomyosin. *J. Muscle Res. Cell Motil.* **38**, 183–191 (2017).
[73] Bottinelli, R., Coviello, D. A., Redwood, C. S., Pellegrino, M. A., Maron, B. J., Spirito, P., *et al*. A mutant tropomyosin that causes hypertrophic cardiomyopathy is expressed *in vivo* and associated with an increased calcium sensitivity. *Circ. Res*. **82**, 106–115 (1998).
[74] Wang, L., Bahadir, A. & Kawai, M. High ionic strength depresses muscle contractility by decreasing both force per cross-bridge and the number of strongly attached cross-bridges. *J. Muscle Res. Cell Motil.* **36**, 227–241 (2015).
[75] Heald, R. W. & Hitchcock-DeGregori, S. E. The structure of the amino terminus of tropomyosin is critical for binding to actin in the absence and presence of troponin. *J. Biol. Chem.* **263**, 5254–5259 (1988).
[76] Urbancikova, M. & Hitchcock-DeGregori, S. E. Requirement of amino-terminal modification for striated muscle alpha-tropomyosin function. *J. Biol. Chem.* **269**, 24310–24315 (1994).
[77] Maytum, R., Konrad, M., Lehrer, S. S. & Geeves, M. A. Regulatory properties of tropomyosin effects of length, isoform, and N-terminal sequence. *Biochemistry* **40**, 7334–7341 (2001).